Journal of Computational Physics **160,** 481–499 (2000)
doi:10.1006/jcph.2000.6466, available online at http://www.idealibrary.com on IDEAL®

A Finite Volume Method for the Approximation of Diffusion Operators on Distorted Meshes

F. Hermeline

CEA/DIF, DCSA/SNEC, BP 12, 91680 Bruyères le Châtel, France

Received June 4, 1999; revised February 3, 2000

A new finite volume method is presented for discretizing general linear or nonlinear elliptic second-order partial-differential equations with mixed boundary conditions. The advantage of this method is that arbitrary distorted meshes can be used without the numerical results being altered. The resulting algorithm has more unknowns than standard methods like finite difference or finite element methods. However, the matrices that need to be inverted are positive definite, so the most powerful linear solvers can be applied. The method has been tested on a few elliptic and parabolic equations, either linear, as in the case of the standard heat diffusion equation, or nonlinear, as in the case of the radiation diffusion equation and the resistive diffusion equation with Hall term.

Key Words: discretization; finite volume method; heat diffusion; resistive diffusion; Hall effect.

1. INTRODUCTION

The numerical modelling in Lagrangian hydrodynamics or magnetohydrodynamics requires the approximation of diffusion operators, possibly with mixed derivatives, without the numerical results being altered by mesh distortions. In order to satisfy this condition several methods have already been proposed [2, 5, 8, 13]. Here we present a new finite volume method which has been briefly described in [7]. This method does not depend on the mesh regularity, but it is suited to approximate mixed derivatives and it degenerates into the finite difference method or the finite element method when the mesh is regular.

Given $\lambda, \boldsymbol{\kappa}$ a positive function and a positive definite matrix, we will focus on the approximation of the model diffusion equation:

$$-\boldsymbol{\nabla} \cdot (\boldsymbol{\kappa} \cdot \boldsymbol{\nabla} u) = f \qquad \text{in } \Omega$$
$$(\boldsymbol{\kappa} \cdot \boldsymbol{\nabla} u) \cdot \boldsymbol{\nu} + \lambda u = g \qquad \text{on } \partial\Omega.$$

The principle of the method lies in the main following steps.

1. Define two meshes on the domain Ω: a primary mesh and a dual mesh.

0021-9991/00 $35.00

2. Integrate the diffusion equation over each cell of both these meshes.

3. Using Green's formula, reduce the integral over one cell to the sum of the fluxes over each side of the cell.

4. Introduce the values of the unknown function u both at the nodes of the primary mesh and at those of the dual mesh as degrees of freedom for correctly approximating the fluxes over the sides.

For simplicity of exposition we will first assume that $\boldsymbol{\kappa}$ is a scalar matrix before handling the general case.

We will present numerical results for one model elliptic equation which enables a comparison with an analytic solution. The numerical experiments on the example of the distorted mesh described in [8] show that the method gives second-order accuracy.

Finally we will present some numerical results for both linear and nonlinear parabolic equations such as heat diffusion, radiation diffusion, and resistive diffusion with Hall effect.

2. DEFINITIONS AND NOTATION

Let Ω be an open bounded polygonal set of R^2 with boundary $\partial\Omega$. We use a mesh on Ω (called primary mesh) made up of arbitrary polygons (in practice triangles or quadrangles). With each (primary) element of this mesh we associate one (primary) point: the centroid is a qualified candidate but other points can be chosen. Similarly, with each boundary side we associate one primary point: the midpoint is the natural candidate. Thus we obtain a set of (primary) points that we connect in order to define a second mesh (called dual mesh: see Fig. 1).

To ease the description we define the nodes of the primary mesh to be dual points. Allowing for this definition the primary (resp. dual) points are the nodes of the dual (resp. primary) mesh and they will be numbered by p (resp. d). The primary polygon sides and their corresponding dual polygon sides will be numbered by s. Furthermore let us denote by (see Fig. 2)

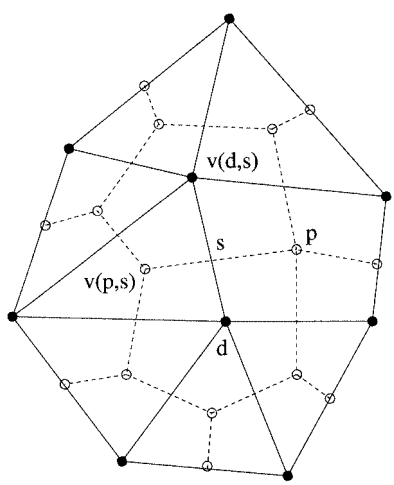

FIG. 1. A sample primary mesh (solid lines) and its dual mesh (dashed lines).

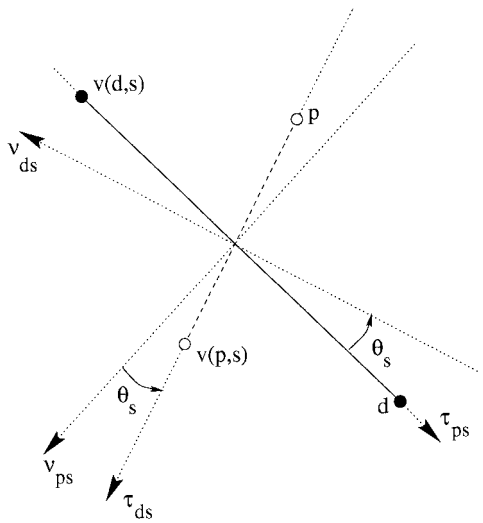

FIG. 2. A sample cross made up with the primary polygon side $S_{ps} = [d, v(d, s)]$ (solid lines) and its corresponding dual polygon side $S_{ds} = [p, v(p, s)]$ (dashed lines).

- $\boldsymbol{\nu}$ the unit outward normal vector and $\boldsymbol{\tau}$ the unit counterclockwise tangent vector on $\partial\Omega$;
- N_P (resp. N_D) the number of primary (resp. dual) points and N_S the number of sides;
- P_p (resp. D_d) the primary (resp. dual) polygon associated with the primary interior point p (resp. the dual point d);
- S_{ps} (resp. S_{ds}) the primary (resp. dual) polygon side number s;
- $\boldsymbol{\nu}_{ps}$ and $\boldsymbol{\nu}_{ds}$ (resp. $\boldsymbol{\tau}_{ps}$ and $\boldsymbol{\tau}_{ds}$) the unit outward normal vector (resp. the unit counterclockwise tangent vector) on the sides S_{ps} and S_{ds} of P_p and D_d;
- $\|P_p\|$ (resp. $\|D_d\|$) the area of P_p (resp. D_d) and $|S_{ps}|$ (resp. $|S_{ds}|$) the length of the side S_{ps} (resp. S_{ds});
- θ_s the angle between $\boldsymbol{\nu}_{ps}$ and $\boldsymbol{\tau}_{ds}$
- $v(p, s)$ (resp. $v(d, s)$) the primary (resp. dual) point connected to p (resp. d) by the dual side S_{ds} (resp. primary side S_{ps}).

Given u a function we will denote by u_p (resp. u_d) the values of u at the primary (resp. dual) points.

3. APPROXIMATION OF THE DIFFUSION OPERATOR: THE SCALAR CASE

Given λ, κ positive functions, consider the model diffusion problem

$$\begin{aligned} -\boldsymbol{\nabla} \cdot (\kappa \boldsymbol{\nabla} u) &= f \qquad \text{in } \Omega \\ \kappa \boldsymbol{\nabla} u \cdot \boldsymbol{\nu} + \lambda u &= g \qquad \text{on } \partial\Omega. \end{aligned} \tag{1}$$

3.1. The Finite Volume Method

Let us make the following operations:

- integrate the first equation over each primary polygon P_p;

- integrate the second equation over each boundary primary side S_{ps};
- integrate the first equation over each dual polygon D_d.

Thus we obtain

$$-\iint_{P_p} \nabla\cdot(\kappa\nabla u) = -\sum_{s\in\partial P_p}\int_{S_{ps}} \kappa\nabla u\cdot\boldsymbol{\nu}_{ps} = \iint_{P_p} f$$

$$\int_{S_{ps}\cap\partial\Omega} \kappa\nabla u\cdot\boldsymbol{\nu}_{ps} + \int_{S_{ps}\cap\partial\Omega}\lambda u = \int_{S_{ps}\cap\partial\Omega} g$$

$$-\iint_{D_d} \nabla\cdot(\kappa\nabla u) = -\sum_{s\in\partial D_d}\int_{S_{ds}} \kappa\nabla u\cdot\boldsymbol{\nu}_{ds} + \int_{D_d\cap\partial\Omega}\lambda u = \iint_{D_d} f + \int_{D_d\cap\partial\Omega} g.$$

By noticing that

$$\boldsymbol{\nu}_{ps} = -\tan\theta_s\boldsymbol{\tau}_{ps} + \frac{1}{\cos\theta_s}\boldsymbol{\tau}_{ds}$$

$$\boldsymbol{\nu}_{ds} = -\frac{1}{\cos\theta_s}\boldsymbol{\tau}_{ps} + \tan\theta_s\boldsymbol{\tau}_{ds}$$

we obtain

$$\begin{aligned}
&-\sum_{s\in\partial P_p}\left(-\tan\theta_s\int_{S_{ps}}\kappa\nabla u\cdot\boldsymbol{\tau}_{ps} + \frac{1}{\cos\theta_s}\int_{S_{ps}}\kappa\nabla u\cdot\boldsymbol{\tau}_{ds}\right) = \iint_{P_p} f\\
&-\tan\theta_s\int_{S_{ps}\cap\partial\Omega}\kappa\nabla u\cdot\boldsymbol{\tau}_{ps} + \frac{1}{\cos\theta_s}\int_{S_{ps}\cap\partial\Omega}\kappa\nabla u\cdot\boldsymbol{\tau}_{ds} + \int_{S_{ps}\cap\partial\Omega}\lambda u = \int_{S_{ps}\cap\partial\Omega} g\\
&-\sum_{s\in\partial D_d}\left(-\frac{1}{\cos\theta_s}\int_{S_{ds}}\kappa\nabla u\cdot\boldsymbol{\tau}_{ps} + \tan\theta_s\int_{S_{ds}}\kappa\nabla u\cdot\boldsymbol{\tau}_{ds}\right) + \int_{D_d\cap\partial\Omega}\lambda u\\
&\quad = \iint_{D_d} f + \int_{D_d\cap\partial\Omega} g.
\end{aligned} \tag{2}$$

Let $\bar{\kappa}_{ps}$ (resp. $\bar{\kappa}_{ds}$) be an average value of κ along the side S_{ps} (resp. S_{ds}); we use the approximations

$$\int_{S_{ps}}\kappa\nabla u\cdot\boldsymbol{\tau}_{ps} \simeq \bar{\kappa}_{ps}\left(u_d - u_{v(d,s)}\right), \qquad \int_{S_{ds}}\kappa\nabla u\cdot\boldsymbol{\tau}_{ds} \simeq \bar{\kappa}_{ds}\left(u_{v(p,s)} - u_p\right)$$

$$\int_{S_{ps}}\kappa\nabla u\cdot\boldsymbol{\tau}_{ds} \simeq \bar{\kappa}_{ps}\frac{|S_{ps}|}{|S_{ds}|}\left(u_{v(p,s)} - u_p\right), \qquad \int_{S_{ds}}\kappa\nabla u\cdot\boldsymbol{\tau}_{ps} \simeq \bar{\kappa}_{ds}\frac{|S_{ds}|}{|S_{ps}|}\left(u_d - u_{v(d,s)}\right)$$

and

$$\iint_{P_p} f \simeq \|P_p\| f_p, \qquad \iint_{D_d} f \simeq \|D_d\| f_d$$

$$\int_{S_{ps}\cap\partial\Omega}\lambda u \simeq |S_{ps}|\lambda_p u_p, \qquad \int_{S_{ps}\cap\partial\Omega} g \simeq |S_{ps}| g_p$$

$$\int_{D_d\cap\partial\Omega}\lambda u \simeq |D_d\cap\partial\Omega|\lambda_d u_d, \qquad \int_{D_d\cap\partial\Omega} g \simeq |D_d\cap\partial\Omega| g_d.$$

Finally, by replacing in the initial equations (2), we obtain the following linear system of $N = N_P + N_D$ equations in N unknowns:

$$\sum_{s\in\partial P_p}\left(\bar{\kappa}_{ps}\tan\theta_s\left(u_d - u_{v(d,s)}\right) + \bar{\kappa}_{ds}\frac{1}{\cos\theta_s}\frac{|S_{ps}|}{|S_{ds}|}\left(u_p - u_{v(p,s)}\right)\right) = \|P_p\| f_p \qquad (p\in\Omega)$$

$$\bar{\kappa}_{ps}\tan\theta_s\left(u_d - u_{v(d,s)}\right) + \bar{\kappa}_{ds}\frac{1}{\cos\theta_s}\frac{|S_{ps}|}{|S_{ds}|}\left(u_p - u_{v(p,s)}\right) + |S_{ps}|\lambda_p u_p = |S_{ps}| g_p \quad (p\in\partial\Omega) \tag{3}$$

$$\sum_{s\in\partial D_d}\left(\bar{\kappa}_{ps}\frac{1}{\cos\theta_s}\frac{|S_{ds}|}{|S_{ps}|}\left(u_d - u_{v(d,s)}\right) + \bar{\kappa}_{ds}\tan\theta_s\left(u_p - u_{v(p,s)}\right)\right) + |D_d\cap\partial\Omega|\lambda_d u_d$$
$$= \|D_d\| f_d + |D_d\cap\partial\Omega| g_d.$$

Note that $N = N_S + N_{BS} + 1 - N_H$ where N_{BS} is the number of boundary sides, and N_H is the number of holes in Ω (see [3], for example).

3.2. Properties of the Matrix of the Linear System

The matrix of the linear system (3) can be written as

$$\mathbf{A} = \begin{pmatrix} \mathbf{B} & \mathbf{U} \\ \mathbf{V} & \mathbf{C} \end{pmatrix},$$

where $\mathbf{B}$ is an $N_P \times N_P$ matrix such that

$$B_{pp} = \sum_{s\in\partial P_p}\bar{\kappa}_{ds}\frac{1}{\cos\theta_s}\frac{|S_{ps}|}{|S_{ds}|} \qquad (p\in\Omega)$$

$$B_{pp} = \bar{\kappa}_{ds}\frac{1}{\cos\theta_s}\frac{|S_{ps}|}{|S_{ds}|} + |S_{ps}|\lambda_p \qquad (p\in\partial\Omega)$$

$$B_{pq} = -\bar{\kappa}_{ds}\frac{1}{\cos\theta_s}\frac{|S_{ps}|}{|S_{ds}|} \qquad (p\neq q = v(p,s));$$

$\mathbf{C}$ is an $N_D \times N_D$ matrix such that

$$C_{dd} = \sum_{s\in\partial D_d}\bar{\kappa}_{ps}\frac{1}{\cos\theta_s}\frac{|S_{ds}|}{|S_{ps}|} + |D_d\cap\partial\Omega|\lambda_d$$

$$C_{de} = -\bar{\kappa}_{ps}\frac{1}{\cos\theta_s}\frac{|S_{ds}|}{|S_{ps}|} \qquad (d\neq e = v(d,s));$$

$\mathbf{U}$ is an $N_P \times N_D$ matrix such that (s and t being the sides of P_p which contain d)

$$U_{pd} = \bar{\kappa}_{ps}\tan\theta_s - \bar{\kappa}_{pt}\tan\theta_t;$$

and $\mathbf{V}$ is an $N_D \times N_P$ matrix such that (s and t being the sides of D_d which contain p)

$$V_{dp} = \bar{\kappa}_{ds}\tan\theta_s - \bar{\kappa}_{dt}\tan\theta_t.$$

Since it is well known that an $\mathbf{M}$-type matrix satisfies a discrete maximum principle, we are interested in conditions for $\mathbf{A}$ to be an $\mathbf{M}$-matrix (see [15]). We recall that $\mathbf{A}$ is an $\mathbf{M}$-matrix if it is irreducible (i.e., the graph corresponding to $\mathbf{A}$ is connected), diagonally

dominant, and

$$A_{ii} > 0 \quad \forall i; \qquad A_{ij} \le 0 \quad \forall i,j \quad i \neq j; \qquad A_{ii} > \sum_{i \neq j} |A_{ij}| \text{ for at least one } j.$$

The matrices **B**, **C** are symmetric **M**-matrices. Unfortunately the matrix **A** itself is not an **M**-matrix, nor is it diagonally dominant, but we can prove that is positive definite.

THEOREM 1. *Suppose that there exists $p, d \in \partial\Omega$ such that $\lambda_p \neq 0, \lambda_d \neq 0$. If for all s, $\bar{\kappa}_{ps} = \bar{\kappa}_{ds}$, then* **A** *is symmetric positive definite. If there exists s such that $\bar{\kappa}_{ps} \neq \bar{\kappa}_{ds}$,* **A** *is no more symmetric but it remains positive definite if the following condition holds*:

$$\frac{1}{4}(\bar{\kappa}_{ps} + \bar{\kappa}_{ds})^2 \sin^2\theta_s < \bar{\kappa}_{ps}\bar{\kappa}_{ds} \qquad \forall s. \tag{4}$$

Proof. By multiplying the equations of the system (3) by u_p and u_d and adding, we obtain

$$\begin{aligned}
&\sum_p \sum_{s \in \partial P_p} \left(\bar{\kappa}_{ps} \tan\theta_s \big(u_d - u_{v(d,s)}\big) u_p + \bar{\kappa}_{ds} \frac{1}{\cos\theta_s} \frac{|S_{ps}|}{|S_{ds}|} \big(u_p - u_{v(p,s)}\big) u_p \right) \\
&\quad + \sum_d \sum_{s \in \partial D_d} \left(\bar{\kappa}_{ps} \frac{1}{\cos\theta_s} \frac{|S_{ds}|}{|S_{ps}|} \big(u_d - u_{v(d,s)}\big) u_d + \bar{\kappa}_{ds} \tan\theta_s \big(u_p - u_{v(p,s)}\big) u_d \right) \\
&\quad + \sum_{p \in \partial\Omega} |S_{ps}| \lambda_p u_p^2 + \sum_{d \in \partial\Omega} |D_d \cap \partial\Omega| \lambda_d u_d^2 \\
&= \sum_p \|P_p\| f_p u_p + \sum_d \|D_d\| f_d u_d + \sum_{p \in \partial\Omega} |S_{ps}| g_p u_p + \sum_{d \in \partial\Omega} |D_d \cap \partial\Omega| g_d u_d.
\end{aligned}$$

The left-hand side of the last formula can be rewritten as

$$\begin{aligned}
&\sum_s \frac{1}{\cos\theta_s} \left(\bar{\kappa}_{ds} \frac{|S_{ps}|}{|S_{ds}|} \big(u_p - u_{v(p,s)}\big)^2 + \bar{\kappa}_{ps} \frac{|S_{ds}|}{|S_{ps}|} \big(u_d - u_{v(d,s)}\big)^2 + (\bar{\kappa}_{ps} + \bar{\kappa}_{ds}) \right. \\
&\quad \left. \times \sin\theta_s \big(u_p - u_{v(p,s)}\big)\big(u_d - u_{v(d,s)}\big) \right) + \sum_{p \in \partial\Omega} |S_{ps}| \lambda_p u_p^2 + \sum_{d \in \partial\Omega} |D_d \cap \partial\Omega| \lambda_d u_d^2
\end{aligned}$$

or

$$\begin{aligned}
&\sum_s \frac{1}{\cos\theta_s} \bar{\kappa}_{ds} \frac{|S_{ps}|}{|S_{ds}|} \left(\left(u_p - u_{v(p,s)} + \frac{1}{2} \frac{\bar{\kappa}_{ps} + \bar{\kappa}_{ds}}{\bar{\kappa}_{ds}} \frac{|S_{ds}|}{|S_{ps}|} \sin\theta_s \big(u_d - u_{v(d,s)}\big) \right)^2 \right. \\
&\quad \left. + \left(\frac{\bar{\kappa}_{ps}}{\bar{\kappa}_{ds}} - \frac{1}{4} \frac{(\bar{\kappa}_{ps} + \bar{\kappa}_{ds})^2}{\bar{\kappa}_{ds}^2} \sin^2\theta_s \right) \frac{|S_{ds}|^2}{|S_{ps}|^2} \big(u_d - u_{v(d,s)}\big)^2 \right) \\
&\quad + \sum_{p \in \partial\Omega} |S_{ps}| \lambda_p u_p^2 + \sum_{d \in \partial\Omega} |D_d \cap \partial\Omega| \lambda_d u_d^2.
\end{aligned}$$

On the one hand, under the assumptions of the theorem, the preceding term is always positive. On the other hand, if for all p, d, $f_p = 0$, $f_d = 0$, $g_p = 0$, and $g_d = 0$ then, for all p, d, $u_p = 0$ and $u_d = 0$. Therefore **A** is positive definite. ∎

In practice we choose

$$\bar{\kappa}_{ps} = \bar{\kappa}_{ds} = \frac{1}{4}\big(\kappa_p + \kappa_d + \kappa_{v(p,s)} + \kappa_{v(d,s)}\big).$$

In this case the theoretical condition (4) is always satisfied.

3.3. Comparison with Other Methods

3.3.1. *Delaunay–Voronoi Meshes*

Suppose that the primary cells are triangles or quadrangles whose vertices are co-circular. We will say that the primary mesh is a so-called Delaunay mesh if and only if the circumcircle of any primary cell does not contain a dual point in its interior (see [4, 11]). If Ω contains these circumcircle centers, they can be chosen as primary points in order to obtain the so-called Voronoi mesh as the dual mesh. Then the (primary) Delaunay mesh and the (dual) Voronoi mesh are such that

$$\theta_s = 0 \qquad \forall s.$$

In this case the linear system (3) degenerates into the two simplest linear systems (we assume that $\kappa = 1$)

$$\begin{aligned} \sum_{s \in \partial P_p} \frac{|S_{ps}|}{|S_{ds}|}\left(u_p - u_{v(p,s)}\right) &= \|P_p\| f_p \\ \frac{|S_{ps}|}{|S_{ds}|}\left(u_p - u_{v(p,s)}\right) + |S_{ps}|\lambda_p u_p &= |S_{ps}| g_p \end{aligned} \tag{5}$$

and

$$\sum_{s \in \partial D_d} \frac{|S_{ds}|}{|S_{ps}|}\left(u_d - u_{v(d,s)}\right) + |D_d \cap \partial\Omega|\lambda_d u_d = \|D_d\| f_d + |D_d \cap \partial\Omega| g_d. \tag{6}$$

We obtain two different methods for approximating to the same diffusion equation (1): the method (5), which can be called the primary method, provides an approximation of the solution at the primary points, whereas the method (6), which can be called the dual method, provides an approximation of the solution at the dual points (see [6, 12]).

When the primary cells are rectangles the method (5) coincides with the standard cell-centered finite difference method. When the primary cells are triangles it is known that the method (6) coincides with the piecewise linear finite element method (see, for example, [9, 10]). In both these cases the matrix that needs to be inverted is an **M**-matrix.

3.3.2. *General Meshes*

When the mesh is made up of arbitrary quadrangles we obtain a nine-point method which can be compared with the quadrilateral finite element method and the methods described in [2, 5, 8, 13], although the degrees of freedom are not the same.

4. APPROXIMATION OF THE DIFFUSION OPERATOR: THE GENERAL CASE

Given λ, a positive function, and $\boldsymbol{\kappa}$, a positive definite matrix, consider now the general model diffusion problem

$$\begin{aligned} -\boldsymbol{\nabla} \cdot (\boldsymbol{\kappa} \cdot \boldsymbol{\nabla} u) &= f \qquad \text{in } \Omega \\ (\boldsymbol{\kappa} \cdot \boldsymbol{\nabla} u) \cdot \boldsymbol{\nu} + \lambda u &= g \qquad \text{on } \partial\Omega. \end{aligned}$$

4.1. The Finite Volume Method

Make the same operations as the ones of the beginning of Subsection 3.1, and notice that

$$(\boldsymbol{\kappa}\cdot\boldsymbol{\nabla}u)\cdot\boldsymbol{\nu}=\boldsymbol{\nabla}u\cdot(\boldsymbol{\kappa}^t\cdot\boldsymbol{\nu});$$

we obtain

$$-\iint_{P_p}\boldsymbol{\nabla}\cdot(\boldsymbol{\kappa}\boldsymbol{\nabla}u)=-\sum_{s\in\partial P_p}\int_{S_{ps}}\boldsymbol{\nabla}u\cdot(\boldsymbol{\kappa}^t\cdot\boldsymbol{\nu}_{ps})=\iint_{P_p}f$$

$$\int_{S_{ps}\cap\partial\Omega}\boldsymbol{\nabla}u\cdot(\boldsymbol{\kappa}^t\cdot\boldsymbol{\nu}_{ps})+\int_{S_{ps}\cap\partial\Omega}\lambda u=\int_{S_{ps}\cap\partial\Omega}g$$

$$-\iint_{D_d}\boldsymbol{\nabla}\cdot(\boldsymbol{\kappa}\boldsymbol{\nabla}u)=-\sum_{s\in\partial D_d}\int_{S_{ds}}\boldsymbol{\nabla}u\cdot(\boldsymbol{\kappa}^t\cdot\boldsymbol{\nu}_{ds})+\int_{D_d\cap\partial\Omega}\lambda u=\iint_{D_d}f+\int_{D_d\cap\partial\Omega}g.$$

Since the vectors $\boldsymbol{\tau}_{ps}$ and $\boldsymbol{\tau}_{ds}$ cannot be collinear, there exists a single $\alpha_s,\beta_s,\gamma_s,\delta_s$, depending on $\boldsymbol{\kappa}$, such that

$$\begin{aligned}\boldsymbol{\kappa}^t\cdot\boldsymbol{\nu}_{ps}&=-\alpha_s(\boldsymbol{\kappa})\boldsymbol{\tau}_{ps}+\beta_s(\boldsymbol{\kappa})\boldsymbol{\tau}_{ds}\\ \boldsymbol{\kappa}^t\cdot\boldsymbol{\nu}_{ds}&=-\gamma_s(\boldsymbol{\kappa})\boldsymbol{\tau}_{ps}+\delta_s(\boldsymbol{\kappa})\boldsymbol{\tau}_{ds},\end{aligned}$$

and we find

$$\begin{aligned}\alpha_s(\boldsymbol{\kappa})&=\frac{1}{\cos\theta_s}\boldsymbol{\nu}_{ds}\cdot(\boldsymbol{\kappa}^t\cdot\boldsymbol{\nu}_{ps})\\ \beta_s(\boldsymbol{\kappa})&=\frac{1}{\cos\theta_s}\boldsymbol{\nu}_{ps}\cdot(\boldsymbol{\kappa}^t\cdot\boldsymbol{\nu}_{ps})\\ \gamma_s(\boldsymbol{\kappa})&=\frac{1}{\cos\theta_s}\boldsymbol{\nu}_{ds}\cdot(\boldsymbol{\kappa}^t\cdot\boldsymbol{\nu}_{ds})\\ \delta_s(\boldsymbol{\kappa})&=\frac{1}{\cos\theta_s}\boldsymbol{\nu}_{ps}\cdot(\boldsymbol{\kappa}^t\cdot\boldsymbol{\nu}_{ds}).\end{aligned}$$

Hence we obtain

$$-\sum_{s\in\partial P_p}\left(-\int_{S_{ps}}\alpha_s(\boldsymbol{\kappa})\boldsymbol{\nabla}u\cdot\boldsymbol{\tau}_{ps}+\int_{S_{ps}}\beta_s(\boldsymbol{\kappa})\boldsymbol{\nabla}u\cdot\boldsymbol{\tau}_{ds}\right)=\iint_{P_p}f$$

$$-\int_{S_{ps}\cap\partial\Omega}\alpha_s(\boldsymbol{\kappa})\boldsymbol{\nabla}u\cdot\boldsymbol{\tau}_{ps}+\int_{S_{ps}\cap\partial\Omega}\beta_s(\boldsymbol{\kappa})\boldsymbol{\nabla}u\cdot\boldsymbol{\tau}_{ds}+\int_{S_{ps}\cap\partial\Omega}\lambda u=\int_{S_{ps}\cap\partial\Omega}g \qquad (7)$$

$$-\sum_{s\in\partial D_d}\left(-\int_{S_{ds}}\gamma_s(\boldsymbol{\kappa})\boldsymbol{\nabla}u\cdot\boldsymbol{\tau}_{ps}+\int_{S_{ds}}\delta_s(\boldsymbol{\kappa})\boldsymbol{\nabla}u\cdot\boldsymbol{\tau}_{ds}\right)+\int_{D_d\cap\partial\Omega}\lambda u=\iint_{D_d}f+\int_{D_d\cap\partial\Omega}g.$$

Let $\overline{\boldsymbol{\kappa}}_{ps}$ (resp. $\overline{\boldsymbol{\kappa}}_{ds}$) be an average (positive definite) value of $\boldsymbol{\kappa}$ along the side S_{ps} (resp. S_{ds}). We use the following approximations:

$$\int_{S_{ps}}\alpha_s(\boldsymbol{\kappa})\boldsymbol{\nabla}u\cdot\boldsymbol{\tau}_{ps}\simeq\alpha_s(\overline{\boldsymbol{\kappa}}_{ps})\left(u_d-u_{v(d,s)}\right)$$

$$\int_{S_{ds}}\beta_s(\boldsymbol{\kappa})\boldsymbol{\nabla}u\cdot\boldsymbol{\tau}_{ds}\simeq\beta_s(\overline{\boldsymbol{\kappa}}_{ds})\left(u_{v(p,s)}-u_p\right)$$

$$\int_{S_{ps}} \gamma_s(\boldsymbol{\kappa}) \boldsymbol{\nabla} u \cdot \boldsymbol{\tau}_{ps} \simeq \gamma_s(\bar{\boldsymbol{\kappa}}_{ps}) \big(u_d - u_{v(d,s)}\big)$$

$$\int_{S_{ds}} \delta_s(\boldsymbol{\kappa}) \boldsymbol{\nabla} u \cdot \boldsymbol{\tau}_{ds} \simeq \delta_s(\bar{\boldsymbol{\kappa}}_{ds}) \big(u_{v(p,s)} - u_p\big)$$

$$\int_{S_{ps}} \beta_s(\boldsymbol{\kappa}) \boldsymbol{\nabla} u \cdot \boldsymbol{\tau}_{ds} \simeq \int_{S_{ps}} \left(\frac{1}{|S_{ds}|} \int_{S_{ds}} \beta_s(\boldsymbol{\kappa}) \boldsymbol{\nabla} u \cdot \boldsymbol{\tau}_{ds} \right) \simeq \beta_s(\bar{\boldsymbol{\kappa}}_{ds}) \frac{|S_{ps}|}{|S_{ds}|} \big(u_{v(p,s)} - u_p\big)$$

$$\int_{S_{ds}} \gamma_s(\boldsymbol{\kappa}) \boldsymbol{\nabla} u \cdot \boldsymbol{\tau}_{ps} \simeq \int_{S_{ds}} \left(\frac{1}{|S_{ps}|} \int_{S_{ps}} \gamma_s(\boldsymbol{\kappa}) \boldsymbol{\nabla} u \cdot \boldsymbol{\tau}_{ps} \right) \simeq \gamma_s(\bar{\boldsymbol{\kappa}}_{ps}) \frac{|S_{ds}|}{|S_{ps}|} \big(u_d - u_{v(d,s)}\big).$$

Finally, by inserting these into the initial system (7), we find the following linear system of $N = N_P + N_D$ equations in N unknowns:

$$\begin{aligned}
&\sum_{s \in \partial P_p} \left(\alpha_s(\bar{\boldsymbol{\kappa}}_{ps}) \big(u_d - u_{v(d,s)}\big) + \beta_s(\bar{\boldsymbol{\kappa}}_{ds}) \frac{|S_{ps}|}{|S_{ds}|} \big(u_p - u_{v(p,s)}\big) \right) = \|P_p\| f_p \qquad (p \in \Omega) \\
&\alpha_s(\bar{\boldsymbol{\kappa}}_{ps}) \big(u_d - u_{v(d,s)}\big) + \beta_s(\bar{\boldsymbol{\kappa}}_{ds}) \frac{|S_{ps}|}{|S_{ds}|} \big(u_p - u_{v(p,s)}\big) + |S_{ps}| \lambda_p u_p = |S_{ps}| g_p \qquad (p \in \partial\Omega) \\
&\sum_{s \in \partial D_d} \left(\gamma_s(\bar{\boldsymbol{\kappa}}_{ps}) \frac{|S_{ds}|}{|S_{ps}|} \big(u_d - u_{v(d,s)}\big) + \delta_s(\bar{\boldsymbol{\kappa}}_{ds}) \big(u_p - u_{v(p,s)}\big) \right) + |D_d \cap \partial\Omega| \lambda_d u_d \\
&\quad = \|D_d\| f_d + |D_d \cap \partial\Omega| g_d.
\end{aligned} \tag{8}$$

4.2. Properties of the Matrix of the Linear System

Let $\mathbf{A}$ be the matrix associated with the linear system (8). We can prove the following theorem, which generalizes Theorem 1.

THEOREM 2. *Suppose that there exists $d \in \partial\Omega$, $p \in \partial\Omega$, such that $\lambda_p \neq 0$, $\lambda_d \neq 0$. If $\boldsymbol{\kappa}$ is symmetric and if, for all s, $\bar{\boldsymbol{\kappa}}_{ps} = \bar{\boldsymbol{\kappa}}_{ds}$, then $\mathbf{A}$ is a symmetric positive definite matrix. Conversely, if $\boldsymbol{\kappa}$ is not symmetric or if there exists s such that $\bar{\boldsymbol{\kappa}}_{ps} \neq \bar{\boldsymbol{\kappa}}_{ds}$, $\mathbf{A}$ remains a positive definite matrix if the following condition holds*:

$$\frac{1}{4} (\alpha_s(\bar{\boldsymbol{\kappa}}_{ps}) + \delta_s(\bar{\boldsymbol{\kappa}}_{ds}))^2 < \beta_s(\bar{\boldsymbol{\kappa}}_{ds}) \gamma_s(\bar{\boldsymbol{\kappa}}_{ps}) \qquad \forall s. \tag{9}$$

Proof. The proof is the same as that of Theorem 1. If $\boldsymbol{\kappa}$ is symmetric and if, for all s, $\bar{\boldsymbol{\kappa}}_{ps} = \bar{\boldsymbol{\kappa}}_{ds}$, the condition (9) is the Cauchy–Schwarz inequality for the inner product associated with the positive definite matrix $\bar{\boldsymbol{\kappa}}_{ds} = \bar{\boldsymbol{\kappa}}_{ps}$. ■

5. NUMERICAL EXPERIMENTS

Let us now present some numerical results that illustrate the behavior of the proposed finite volume method.

The symmetric linear systems are solved by the conjuguate gradient method. The non-symmetric linear system is solved by the quasi-minimized conjuguate gradient squared method (see [14]).

Let Ω be the unit square and let $\partial\Omega_S$, $\partial\Omega_E$, $\partial\Omega_N$, $\partial\Omega_W$ be the boundaries of Ω. In order to assess the accuracy of the method we will need the following for several meshes:

1. four regular grids from the coarsest (100 squares of size 0.1) to the finest (6400 squares of size 0.0125);
2. four distorted quadrilateral meshes as the one used in [8] from the coarsest (Fig. 3: 110 quadrangles of average size 0.1) to the finest (5760 quadrangles of average size 0.0125);
3. four distorted triangular meshes which have been constructed by dividing each element of the preceding quadrilateral meshes into four triangles: then we obtain four triangular meshes from the coarsest (Fig. 3: 440 triangles of average size 0.1) to the finest (23040 triangles of average size 0.0125).

5.1. One Linear Elliptic Equation

In order to test the method, consider the following linear elliptic equation whose analytic solution is $u = 2 + \cos(\pi x) + \sin(\pi y)$:

$$\begin{aligned} -\boldsymbol{\nabla}\cdot(\boldsymbol{\nabla}u) &= \pi^2(\cos(\pi x)+\sin(\pi y)) && \text{in } \Omega \\ u &= 2+\cos(\pi x) && \text{on } \partial\Omega_S \cup \partial\Omega_N \\ \boldsymbol{\nabla}u\cdot\boldsymbol{\nu} &= 0 && \text{on } \partial\Omega_E \cup \partial\Omega_W. \end{aligned}$$

Figures 4 and 5 display the error between the exact solution and the computed solution for the above-mentioned meshes. These results call for the following comments.

- The proposed finite volume method is second-order accurate.
- In the case of distorted quadrilateral meshes, the error is similar to the one obtained by using an equivalent regular grid (i.e., if the finite difference method has been used).
- In the case of distorted triangular meshes the proposed finite volume method provides results which are more accurate than those obtained by the piecewise linear finite element method. Let us recall that the error for the piecewise linear finite element method depends on the parameter

$$\sup_{1\le p\le N_P}\left(\frac{d(P_p)}{\rho(P_p)}\right),$$

where $d(P_p)$ is the diameter of P_p, and $\rho(P_p)$ is the diameter of the inscribed circle of P_p (see [1]). It seems that this is not the case for our method.
- We point out that both incomplete finite volume methods that we obtain by taking (see Subsection 3.2)

$$\mathbf{A} = \begin{pmatrix} \mathbf{B} & \mathbf{0} \\ \mathbf{0} & \mathbf{C} \end{pmatrix}$$

do not converge when the mesh is distorted.

In comparison with the piecewise linear finite element method only a moderate number of additional iterations are needed. Tables I and II give the number of iterations for the four triangular distorted meshes mentioned above.

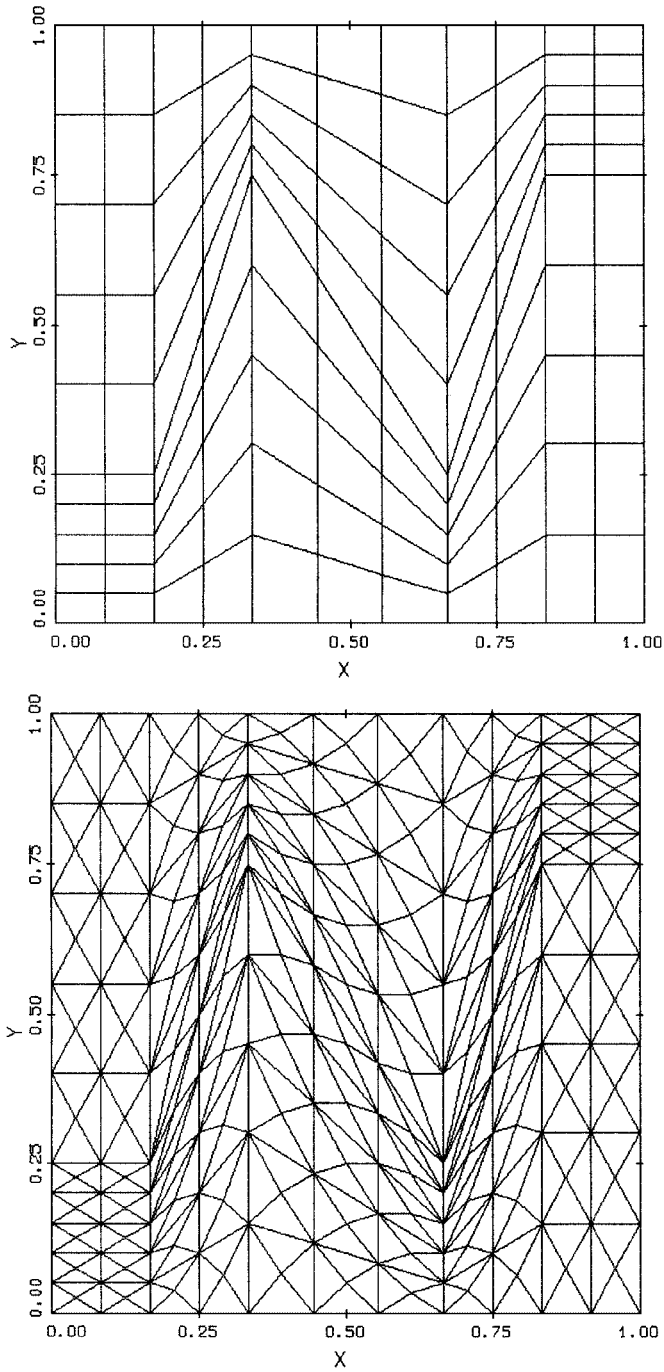

FIG. 3. Quadrilateral and triangular coarse meshes.

TABLE I
Piecewise Linear Finite Element Method

	Number of iterations	Number of unknowns
Mesh 1	75	242
Mesh 2	141	759
Mesh 3	289	2957
Mesh 4	579	11673

TABLE II
Proposed Finite Volume Method

	Number of iterations	Number of unknowns
Mesh 1	163	724
Mesh 2	312	2275
Mesh 3	618	8869
Mesh 4	1230	35017

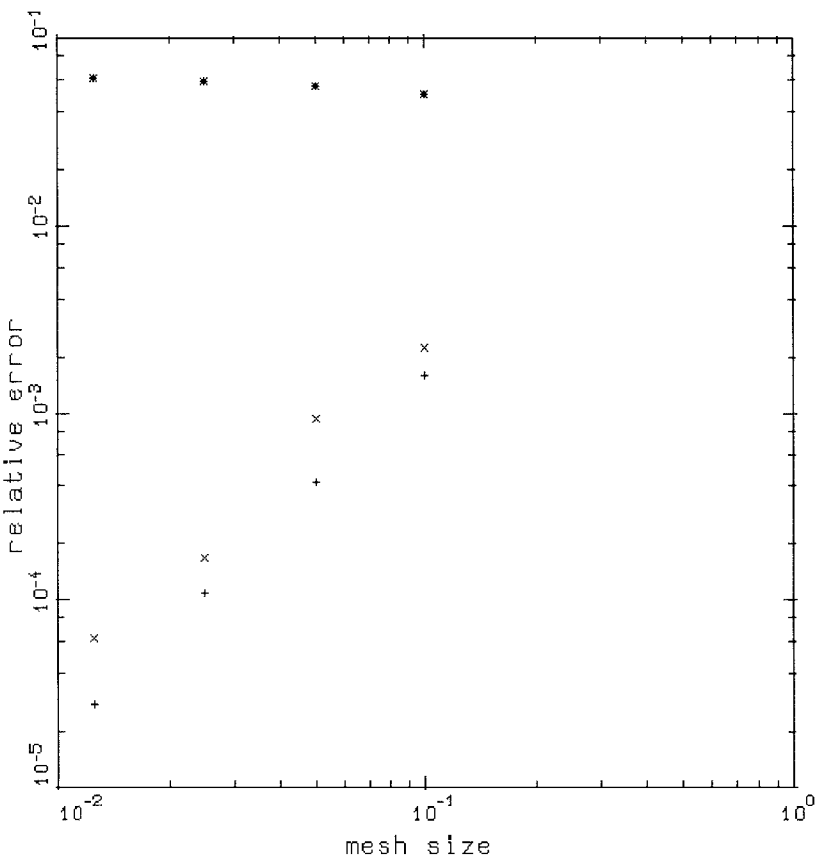

FIG. 4. Relative error between the exact solution and the computed solution for the four distorted quadrilateral meshes: $+$, finite difference method (in this case the distorted mesh is replaced by an equivalent regular grid); $*$, incomplete proposed finite volume method; $\times$, proposed finite volume method.

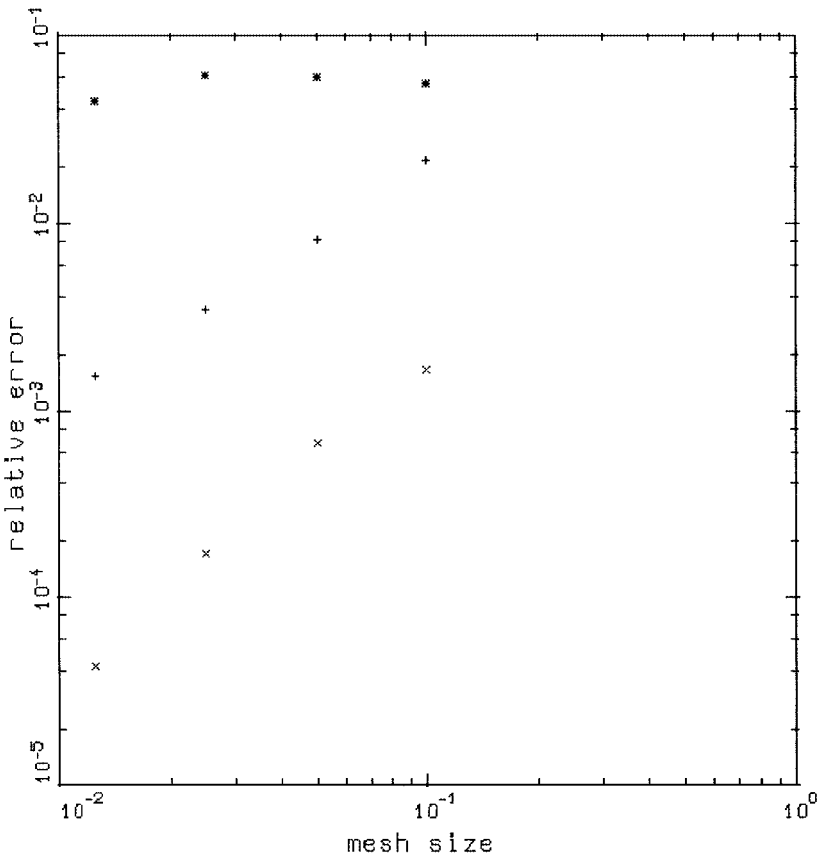

FIG. 5. Relative error between the exact solution and the computed solution for the four distorted triangular meshes: +, piecewise linear finite element method; ∗, incomplete proposed finite volume method; ×, proposed finite volume method.

5.2. One Linear Parabolic Equation

In this subsection we deal with the heat diffusion equation (κ is the thermal conductivity):

$$\begin{aligned} \frac{\partial T}{\partial t} - \boldsymbol{\nabla} \cdot (\kappa \boldsymbol{\nabla} T) &= 0 \qquad \text{in } \Omega \\ T(0) &= T_0 \qquad \text{in } \Omega \\ \kappa \boldsymbol{\nabla} T \cdot \boldsymbol{\nu} + g(T - T_N) &= 0 \qquad \text{on } \partial\Omega_N \\ \kappa \boldsymbol{\nabla} T \cdot \boldsymbol{\nu} &= 0 \qquad \text{on } \partial\Omega_S \cup \partial\Omega_E \cup \partial\Omega_W. \end{aligned}$$

We have chosen $\kappa = 1$, $g = 1$, $T_N = 30$, $T_0 = 1$, and $\Delta t = 5 \times 10^{-4}$, and we have used the finest regular grid and the finest distorted quadrilateral mesh mentioned above. Figure 6 displays the temperature at time $t = 4.10^{-2}$.

5.3. Two Nonlinear Parabolic Equations

In this subsection we deal with two plasma physics problems which can be written as the following nonlinear parabolic equation:

$$\frac{\partial u}{\partial t} - \boldsymbol{\nabla} \cdot (\boldsymbol{\kappa}(u) \cdot \boldsymbol{\nabla} u) = 0.$$

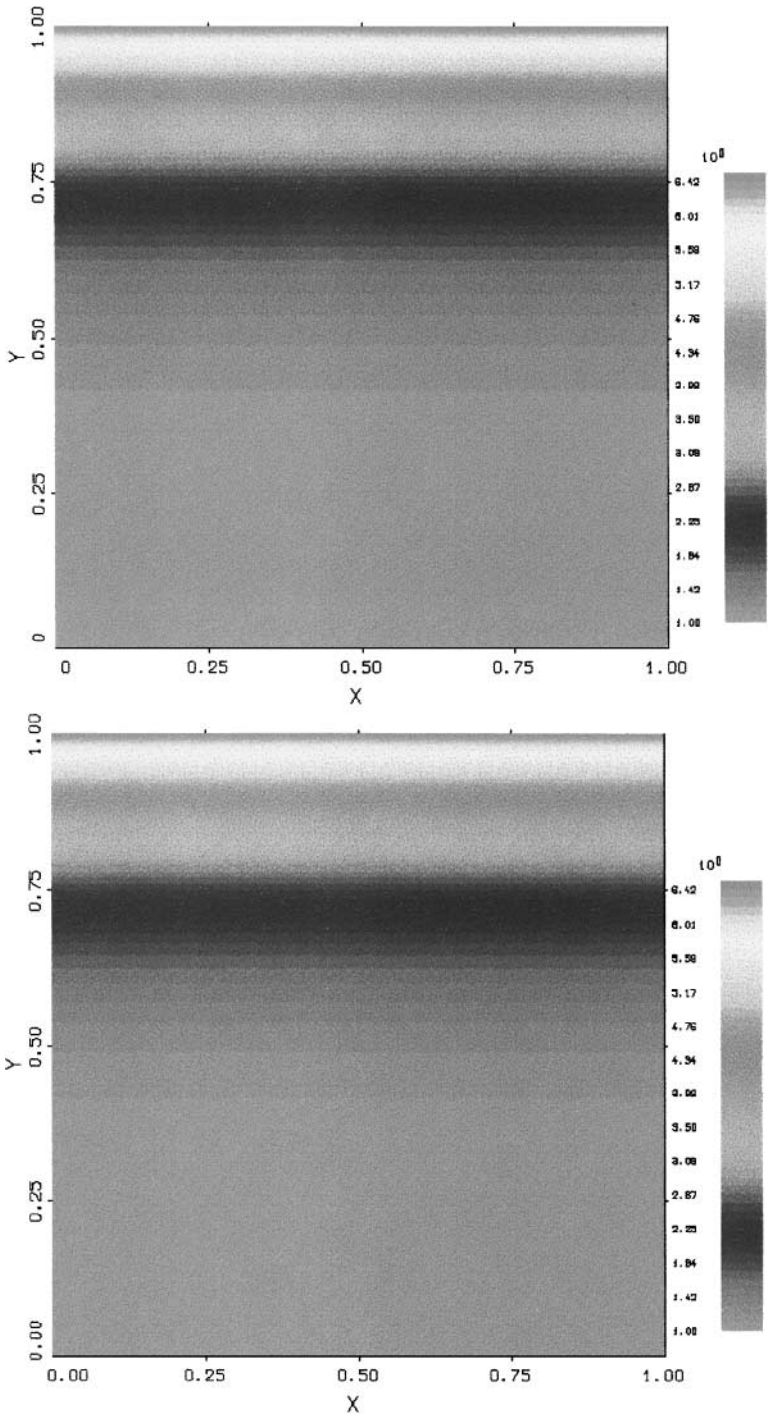

FIG. 6. Temperature at time $t = 4.10^{-2}$ (top, regular grid; bottom, distorted quadrilateral mesh).

We will use the rough implicit time discretization:

$$\frac{u^{n+1}-u^n}{\Delta t} - \nabla \cdot (\kappa(u^n) \cdot \nabla u^{n+1}) = 0$$

At every time step we will enforce the maximum principle by replacing u_p^n and u_d^n by $\sup(u_p^n, u_{\inf}^0)$ and $\sup(u_d^n, u_{\inf}^0)$, where

$$u_{\inf}^0 = \inf_{x\in\Omega}(u^0(x)).$$

We will denote by c, ε_0, μ_0, q_e, m_e, n, and T the light velocity, the permittivity and the permeability of the free space, the charge and the mass of the electron, the density, and the temperature of the plasma. We will use SI units.

5.3.1. *Radiation Diffusion*

In this subsection we deal with the radiation diffusion equation

$$\begin{aligned}
\frac{1}{c}\frac{\partial T^4}{\partial t} - \nabla \cdot (\lambda \nabla T^4) &= 0 \qquad && \text{in } \Omega \\
T(0) &= T_0 \qquad && \text{in } \Omega \\
\lambda \nabla T^4 \cdot \nu + T^4 - T_N^4 &= 0 \qquad && \text{on } \partial\Omega_N \text{ (Marshak condition)} \\
\lambda \nabla T \cdot \nu &= 0 \qquad && \text{on } \partial\Omega_S \cup \partial\Omega_E \cup \partial\Omega_W,
\end{aligned} \tag{10}$$

where

$$\lambda = 1.6 \times 10^{34} \frac{1}{n^2} T^{7/2}$$

Choose T_r as a unit of temperature and let λ_r, t_r be length and time units such as

$$\lambda_r = 1.6 \times 10^{34} \frac{1}{n^2} T_r^{7/2}$$

$$t_r = \frac{\lambda_r}{c}.$$

Let $u = T^4/T_r^4$ and $\kappa(u) = u^{7/8}$; the system (10) becomes

$$\begin{aligned}
\frac{\partial u}{\partial t} - \nabla \cdot (\kappa(u) \nabla u) &= 0 \qquad && \text{in } \Omega \\
u(0) &= u_0 \qquad && \text{in } \Omega \\
\kappa(u) \nabla u \cdot \nu + u - u_N &= 0 \qquad && \text{on } \partial\Omega_N \\
\kappa(u) \nabla u \cdot \nu &= 0 \qquad && \text{on } \partial\Omega_S \cup \partial\Omega_E \cup \partial\Omega_W.
\end{aligned}$$

We have chosen $u_N = 8.1 \times 10^5$, $u_0 = 1$ (hence $T_N = 30 T_r$, $T_0 = T_r$), $\Delta t = 5 \times 10^{-6} t_r$ and we have used the finest regular grid and the finest distorted quadrilateral mesh mentioned above. Figure 7 displays the temperature at time $t = 5 \times 10^{-4} t_r$.

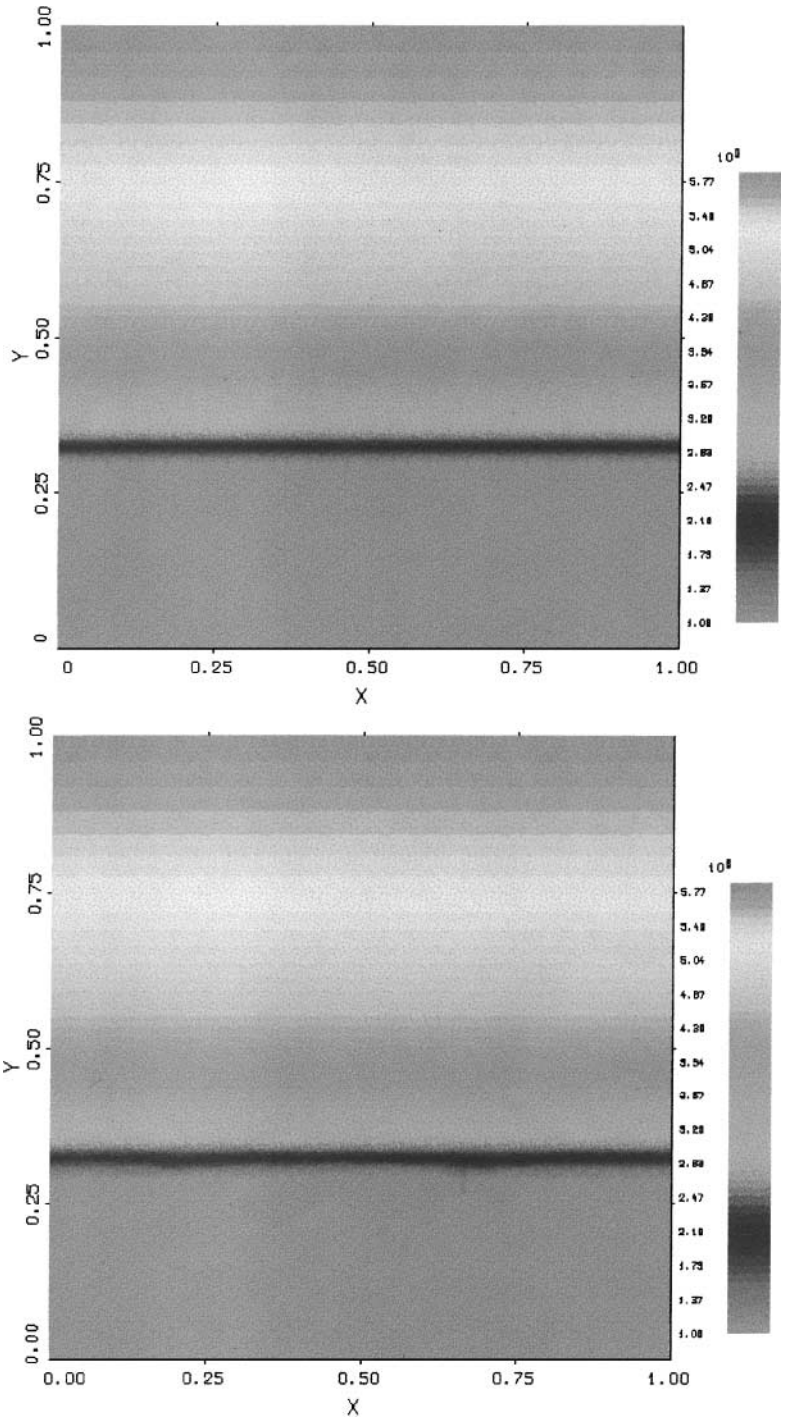

FIG. 7. Temperature T/T_r at time $t = 5.10^{-4}\ \lambda_r/c$ (top, regular grid; bottom, distorted quadrilateral mesh).

5.3.2. *Resistive Diffusion and Hall Effect*

In this subsection, we deal with the resistive diffusion equation with Hall term ($B = B_z$ is the z-component of the magnetic field, σ is the electrical conductivity):

$$\begin{aligned} \frac{\partial B}{\partial t} - \frac{1}{\mu_0}\boldsymbol{\nabla}\cdot\left(\frac{1}{\sigma}\boldsymbol{\nabla}B\right) - \frac{1}{|q_e|\mu_0}\nabla\times\left(\frac{1}{n}B\boldsymbol{\nabla}B\right) &= 0 \qquad \text{in } \Omega \\ B(0) &= B_0 \qquad \text{in } \Omega \\ B &= B_N \qquad \text{on } \partial\Omega_N \\ \boldsymbol{\nabla}B\cdot\boldsymbol{\nu} &= 0 \qquad \text{on } \partial\Omega_S \cup \partial\Omega_E \cup \partial\Omega_W. \end{aligned} \tag{11}$$

Choose n_r as a unit of density and let λ_r, t_r, B_r be length, time, and magnetic field units such that

$$\begin{aligned} \lambda_r &= ct_r \\ t_r &= \omega_p^{-1} = \left(\frac{n_r|q_e|^2}{\varepsilon_0 m_e}\right)^{-1/2} \qquad (\omega_p \text{ is the plasma frequency}) \\ B_r &= \frac{m_e}{|q_e|t_r}. \end{aligned}$$

Let $u = B/B_r$ and

$$\boldsymbol{\kappa}(u) = \begin{pmatrix} \dfrac{\varepsilon_0\omega_p}{\sigma} & \dfrac{n_r}{n}u \\ -\dfrac{n_r}{n}u & \dfrac{\varepsilon_0\omega_p}{\sigma} \end{pmatrix};$$

the system (11) becomes

$$\begin{aligned} \frac{\partial u}{\partial t} - \boldsymbol{\nabla}\cdot(\boldsymbol{\kappa}(u)\boldsymbol{\nabla}u) &= 0 \qquad \text{in } \Omega \\ u(0) &= u_0 \qquad \text{in } \Omega \\ u &= u_N \qquad \text{on } \partial\Omega_N \\ \boldsymbol{\nabla}u\cdot\boldsymbol{\nu} &= 0 \qquad \text{on } \partial\Omega_S \cup \partial\Omega_E \cup \partial\Omega_W. \end{aligned}$$

We have chosen $u_N = -1$, $\Delta t = 5\times 10^{-3}t_r$, and

$$\begin{aligned} u_0 &= -1 \quad \text{if } y \geq 0.5 \quad \text{and} \quad u_0 = 0 \quad \text{if } y < 0.5 \\ \frac{\varepsilon_0\omega_p}{\sigma} &= 10^{-2} \quad \text{if } x \leq 0.5 \quad \text{and} \quad \frac{\varepsilon_0\omega_p}{\sigma} = 10^{-3} \quad \text{if } x > 0.5 \\ \frac{n_r}{n} &= 10^{-1} \quad \text{if } x \leq 0.5 \quad \text{and} \quad \frac{n_r}{n} = 10^{-5} \quad \text{if } x > 0.5 \end{aligned}$$

We have used the finest regular grid and the finest distorted quadrilateral mesh mentioned above. Figure 8 displays the magnetic field at time $t = 0.5t_r$. The results are similar to the ones obtained by a transport-projection method (see [16]).

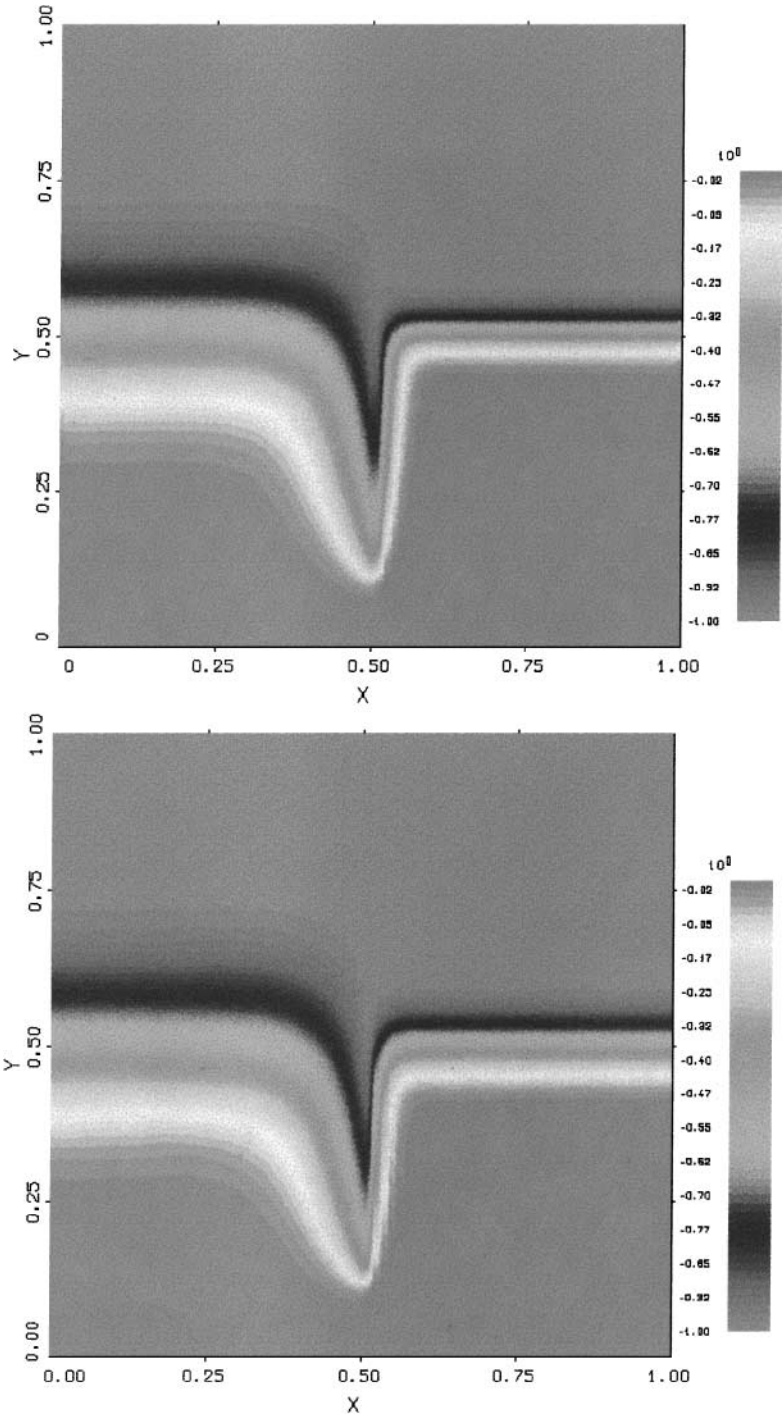

FIG. 8. Magnetic field $B(|q_e|\omega_p^{-1}/m_e)$ at time $t = 0.5\omega_p^{-1}$ (top, regular grid; bottom, distorted quadrilateral mesh).

6. CONCLUSIONS

The numerical experiments show the efficiency of the method. Although no proof has been given, we notice that it is second-order accurate. Furthermore it does not depend on the mesh regularity, unlike the triangular or quadrilateral finite elements, which was the initial objective. In the case of nonlinear problems, however, we observe that it does not verify the maximum principle, without this deficiency being severely penalizing. Actually it suffices to force the calculated solution to respect this principle at every time step to obtain satisfactory results, although the total energy is not exactly preserved.

Allowing for the properties of our finite volume method—its independence from the mesh regularity, its degeneration into the finite difference method on regular grids, its natural adaptation to the discretization of mixed derivatives terms, its easy implementation, and the variety of successfully tested numerical examples—it thus seems to be a qualified candidate for the approximation of diffusion operators on distorted meshes.

REFERENCES

1. P. G. Ciarlet, *The Finite Element Method for Elliptic Problems* (North-Holland, Amsterdam, 1978).
2. I. Faille, A control volume method to solve an elliptic equation on a two-dimensional irregular meshing, *Comput. Meth. Appl. Mech. Eng.* **100**, 275 (1992).
3. D. J. Ewing, A. F. Fawkes, and J. R. Griffiths. Rules governing the numbers of nodes and elements in a finite element mesh, *Int. J. Num. Meth. Eng.* **2**, 597 (1970).
4. P. L. George and H. Borouchaki, *Triangulation de Delaunay et maillage* (Hermes, Paris, 1997).
5. J. E. Morel, J. E. Dendy, M. L. Hall, and S. W. White, A cell centered Lagrangian-mesh diffusion differencing scheme, *J. Comput. Phys.* **103**, 286 (1992).
6. F. Hermeline, Two coupled particle-finite volume methods using Delaunay–Voronoi meshes for the approximation of Vlasov–Poisson and Vlasov–Maxwell equations, *J. Comput. Phys.* **106**, (1993).
7. F. Hermeline, Une méthode de volumes finis pour les équations elliptiques du second ordre, *C. R. Acad. Sci. Paris* **326**, 1433 (1998).
8. D. S. Kershaw, Differencing of the diffusion equation in Lagrangian hydrodynamic codes, *J. Comput. Phys.* **39**, 375 (1981).
9. P. Lascaux and R. Theodor, *Analyse numérique matricielle appliquée à l'art de l'ingénieur* (Masson, Paris, 1986).
10. F. W. Letniowski, Three-dimensional delaunay triangulations for finite element approximations to a second-order diffusion operator, *SIAM J. Sci. Statist. Comput.* **13**, 765 (1992).
11. M. Overmars, M. de Berg, M. van Kreveld, and O. Schwarzkopf, *Computational Geometry* (Springer-Verlag, Berlin/New York, 1997).
12. R. H. MacNeal, An asymmetric finite difference network, *Q. Appl. Math.* **11**, 295 (1953).
13. M. Shashkov and S. Steinberg, Support-operator finite-difference algorithms for general elliptic problems, *J. Comput. Phys.* **118**, 131 (1995).
14. C. H. Tong, A comparative study of preconditioned Lanczos methods for non symmetric linear systems, Sandia Report SAND91-8240 UC-404, Jan. 1992, unpublished.
15. R. S. Varga, *Matrix Iterative Analysis* (Prentice Hall, New York, 1962).
16. V. V. Vikhrev and O. Z. Zabaidullin, Magnetic field spreading along plasma interface due to the Hall effect, *Plasma Phys. Rep.* **20**, 867 (1994).